Evolution of self-organized spin domains under light in single-crystalline $[Fe(ptz)_6](BF_4)_2$

C. Chong, F. Varret, and K. Boukheddaden*
Groupe d'Etudes de la Matière Condensée (GEMaC), CNRS–Université de Versailles, 45 Avenue des Etats Unis, F-78035 Versailles Cedex, France

(Received 15 July 2009; revised manuscript received 23 October 2009; published 8 January 2010)

We study domain growth upon the light-induced phase separation (LIPS) in the spin-crossover $[Fe(ptz)_6](BF_4)_2$ single crystal under clarified conditions of intensity of light and temperature. Our primary motivation is to model the relaxation behavior of a spin-crossover system under light in the spinodal regime. At this end, we built a discrete spatiotemporal hierarchy of coupled equations, which can be regarded as an efficient scheme for simulating the phase separation under light as well as for obtaining the equilibrium mean-field solutions of lattice models having complex structures. We found that in the spinodal regime under light, initial homogeneous states self-organize into spin domains after some incubation time. The evolution patterns of the high- and low-spin domains revealed that the self-organization proceeds roughly in two regimes, viz. diffusion of interfaces in the early stage followed by a growth regime. The analysis of the correlation function shows that the characteristic domain size behaves as $R(t) \sim t^{1/2}$, following the Allen-Cahn law.

DOI: 10.1103/PhysRevB.81.014104 PACS number(s): 64.70.qd, 05.70.Ln, 47.50.Gj, 47.54.−r

I. INTRODUCTION

The photoinduced phase transition (PIPT) has recently attracted a great interest in condensed matter. A large variety of PIPTs have been reported in literature, such as bidirectional photoswitching in single crystals of polydiacetylenes,[1] photoinduced metal-to-insulator transition,[2,3] or neutral to ionic phase transition in tetrathafulvalene-p-chloranyl solids,[4] photoinduced magnetization changes in Prussian blue analogs (cobalt-cynanides),[5–8] light-induced colossal magnetoresistance changes,[9] light-driven isomerization transformations from and ordered to a disordered state,[10] and so on. In these phenomena the effect of light results in a change in the physical properties at the macroscopic scale, through an important role of the electron-lattice (or charge and orbital degrees of freedom) interaction,[11–14] and the behaviors of the related materials are crucially influenced by the competition or the coexistence of multiple phases. The interaction also triggers the observed nonlinear photoexcitation processes and the cooperative dynamics, usually evidenced by the presence of incubation regime in the photoexcitation process and phase separation or spinodal decomposition[15–18] during their subsequent development under light.

Among the photosensitive materials, the spin-crossover (SC) (Refs. 19–29) complexes belong to the category of molecular solids which show under various constraints, such as temperature variations,[19] pressure,[20–22] light irradiation,[23–27] or magnetic field,[28] a transition between the low-spin (LS, $t_{2g}^6 e_g^0$) and the high-spin (HS, $t_{2g}^4 e_g^2$) states.[29,30] For example, Fe(II) SC materials[31] are diamagnetic ($S=0$, LS) and paramagnetic ($S=2$, HS) in the low- and high-temperature phases, respectively. Upon the spin-crossover transition, these materials undergo drastic variations of the metal-ligand bond lengths ($\simeq 0.2$, i.e., $\simeq 10\%$) and ligand-metal-ligand angles (0.5–8°),[24,32] accompanied by important changes in the electronic (spin-state) structure and orbital occupancy. It results in appreciable changes in optical[23,33,34] and magnetic[35–38] properties, offering, then serious potentialities to be integrated in future optical data storage media or to be used as displays.[39–41] In addition, in many cases, elastic interactions between the SC units are strong enough so as to induce hysteresis at the thermal spin transition[42] which then occurs as a first-order phase transition.

Since the discovery of the so-called LIESST (light-induced excited spin state trapping) effect[43–45] in SC materials, the SC complexes become textbook examples of photoswitchable solids. The optical switching (direct or reverse LIESST) is realized at low temperature using different wavelengths for the back and forth processes. The competition between the optical and the thermal processes at low temperature in cooperative materials led to the concept of light-induced instability,[46] from which originates the so-called light-induced thermal hysteresis[47] (LITH) and light-induced optical hysteresis (LIOH) (Refs. 46 and 48) reported some years ago.

The use of these materials as memories for data storage requires however the control of the photo- or the thermoinduced elastic (or magnetoelastic) domains as well as the understanding of the physical mechanisms governing their occurrence. Phase separation was reported long time ago at the thermal spin transition in SC solids,[49] while photoinduced phase separation was only recently observed.[50–57] In most of the experiments however, the phase separation is reported[50,56,58] upon photoexcitation of the solid, i.e. in the metastable photoinduced state. In the case of the highly cooperative SC solid $Fe(btr)_2(NCS)_2H_2O$(btr =4,4bis1,2,4triazole), where the mechanism and kinetics of thermally and light-induced spin transition have been investigated by single-crystal x-ray diffraction techniques, it was evidenced by Pillet *et al.*[58] that the nucleation, growth, and coarsening mechanism of the photoinduced structural domains follow the Avrami model.[59,60] Similar studies[52] have been carried out on the very well documented title compound $[Fe(ptz)_6](BF_4)_2$ in the quenched rhombohedral phase, which is strongly cooperative. Remarkably, $[Fe(ptz)_6](BF_4)_2$ does not show phase transition when the photoinduced phase transition is performed at low temperature.[61] However, Moritomo *et al.*[53] observed a clear evidence of phase separation

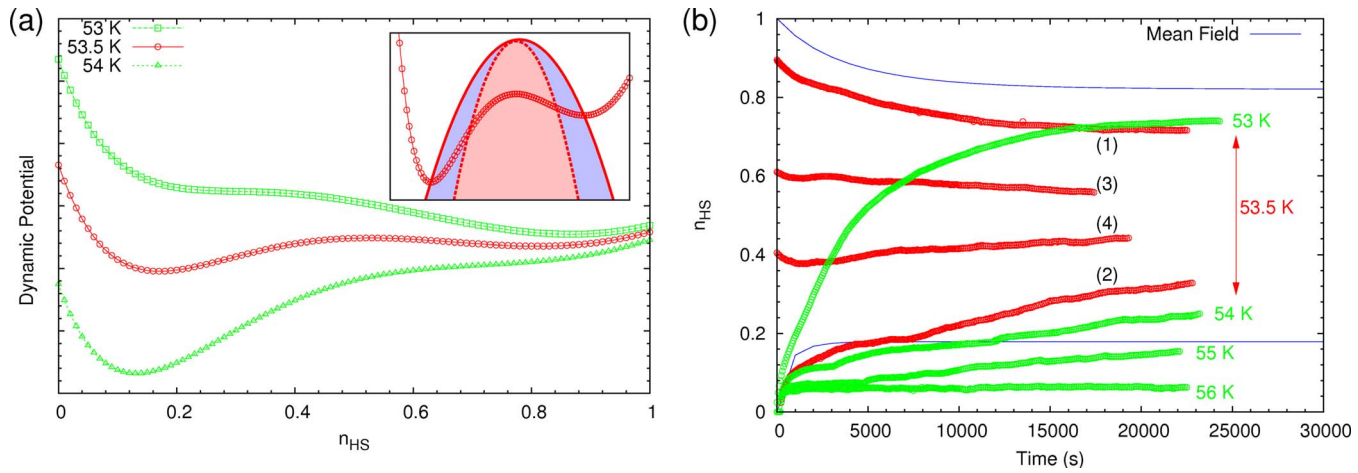

FIG. 1. (Color online) (a) The dynamic potential associated with a bistable situation of the system under permanent irradiation, calculated at different temperatures. In inset, the spinodal area is depicted by the light-red area. The light-blue region represents the ″metastable″ phase. (b) Experimental time dependence of the HS fraction of $[Fe(ptz)_6](BF_4)_2$ starting from inside the LITH loop at 53.5 K, and at neighboring temperature curves (3) and (4) are associated to phase-separation regime after Ref. 51. The blue curves define the mean-field steady states.

upon intense pulse laser excitation above 90 K. Moreover, the relaxation behavior of the photoinduced HS state in $[Fe(ptz)_6](BF_4)_2$ follows the mean-field description, which allows consideration of this system as a prototype for simple theoretical investigations.

From the theoretical side, realistic models[62,63] in which the interaction between the SC complexes is mediated by the lattice distortion have been addressed the problem of the macroscopic phase separation upon the photoexcitation from the LS to the HS state. Based on Monte Carlo simulations on a model introducing the volume striction effects (a constraint which fixes the total volume of the system), Sakai *et al.*[62,63] showed the existence of threshold intensity and incubation period, where the latter corresponds to the nucleation time of the HS domains. To the best of our knowledge, there is no experimental study on the phase separation in the spinodal regime, neither on the time dependence of the characteristic domain size even in the recent elastic model[64–66] investigating thermo- and photoinduced SC transition. In the present study, we mainly focus on the theoretical description of the phase separation in the specific situation of the spinodal regime, occurring in the very narrow thermal region of the LITH loop, under instability conditions.

The paper is organized as follows: in Sec. II we recall the basic aspects of the light-induced phase separation; Sec. III is devoted to the coupled map model; in Sec. IV we present the obtained results on phase separation and discuss their relevance in relation with available data of literature. In Sec. IV we end with a conclusion and perspectives of this work.

II. LIGHT INDUCED PHASE SEPARATION: BASIC CONSIDERATIONS

The observation of the LIPS effect needs to be in presence of LITH loop and one of the most severe conditions of its realization consists in the presence of a slow dynamics. These aspects have been well investigated experimentally (by magnetic measurements) and discussed so far in the case of $[Fe(ptz)_6](BF_4)_2$,[51] yielding the results summarized in Figs. 1(a) and 1(b) in which are depicted the dynamical potential and the time dependence of the HS fraction in the spinodal region.

In particular, Fig. 1(b) illustrates the time dependence of the HS fraction under light at the best working temperature of the spinodal decomposition (T=53.5 K) and at neighboring temperatures. It is clearly observed the existence of two steady states at 53.5 K labeled (1) and (2), corresponding to rich-HS and rich-LS phases, with the respective concentrations n_{HS}=0.8 and $n_{HS}\approx$0.2. In contrast, the curves labeled (3) and (4), prepared in the vicinity of the LIPS effect, evolve with almost (up to fluctuations) invariant HS fractions. In such case a subtle balance takes place between the photoexcitation and the relaxation processes, leading to slow down the dynamics, thus allowing to build up the elastic and electronic correlations which give rise to phase separation. As a consequence, the HS fraction remains macroscopically constant, thus keeping its initial value (here n_{HS}=0.6 or 0.4) while the system fluctuates microscopically. This behavior reminds the spinodal decomposition of binary A-B solids where the order parameter is conserved, although the microscopic mechanism of the phase separation in such a case proceeds via diffusion processes due to the mobility of the atoms.

A simple description of the LITH instability is provided by macroscopic master equation (1),[46,67] based on the homogeneous mean-field approach, which combines light and thermal relaxation processes as

$$\frac{dn_{HS}(t,T)}{dt} = I_0\sigma_0(1-n_{HS}) - n_{HS}k_\infty e^{-E_a/k_BT}e^{-\alpha n_{HS}}$$

$$= -\frac{dU(n_{HS},T)}{dn_{HS}}. \quad (1)$$

Where, E_a is an effective energy barrier, k_∞, the rate constant, $I_0\sigma_0$, the intensity of light, α=J/k_BT (with J the effective interaction between the SC molecules and k_B the Boltzmann

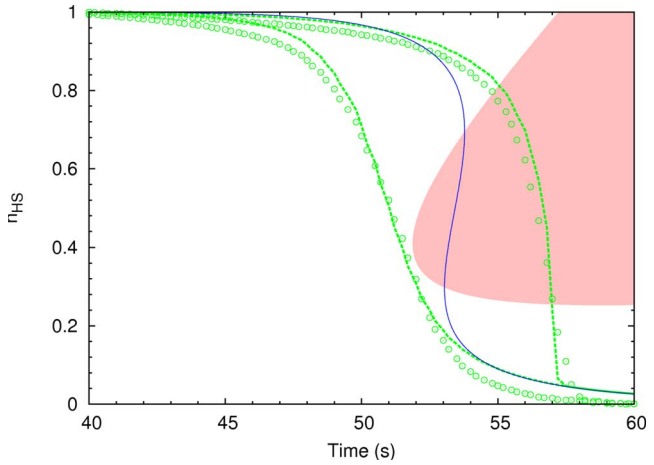

FIG. 2. (Color online) Experimental (○) and theoretical (full and dashed line) light-induced thermal hysteresis loop of $[Fe(ptz)_6](BF_4)_2$ under constant irradiation, 450 nm, 7 mW/cm^2, after Ref. 51. The full blue line is the quasistatic limit of the LITH loop and the dashed green line is the LITH loop obtained using the experimental scan rate 0.035 K/min. The light-red area corresponds to light-induced spinodal instability region. The steady-state values of the HS fraction are $n_{HS} \simeq 0.2$ and $n_{HS} \simeq 0.8$. The transition temperature of the static hysteresis loop is $T_{eq} \approx 53.5$ K.

constant), T the temperature and U the dynamical potential. The best parameter values allowing to reproduce the experimental LITH loop of Fig. 2 are: $I_0\sigma_0 = 5.510^{-4}$ s^{-1}, $k_\infty = 1.510^{-3}$ s^{-1}, $E_a = 663.5$ K, and the effective interaction parameter $J \approx 251.5$ K.

Due to the homogeneous mean-field character of Eq. (1), the subsequent macroscopic dynamical potential only provides the macroscopic steady states and the spinodals of the system, between which phase separation occurs, as depicted in Fig. 3(a). It, of course, does not provide any description of the phase separation evidenced by experimental data [curves (3) and (4)] of Fig. 1(b). Indeed, the stabilization of intermediate states during relaxation under light is an indication of spontaneous pattern formation, in which probably the growth is limited by the slow relaxation and the existence of pinning centers around the defects of the crystal.

One interesting feature of the dynamical potential concept lies with the possibility to derive the phase diagram of the system, shown here in the inset of Fig. 1(a). Similarly to the case of binary mixtures (liquid or alloy), where the order parameter is the miscibility gap, it is possible to define an effective "driving force" as $\mu(n_{HS}) = \frac{\partial U}{\partial n_{HS}}$.

Around the central temperature of the LITH loop, there are two stable steady states, $n_1^\star(T) \simeq 0.8$, and $n_2^\star(T) \simeq 0.2$, respectively, denoting the "HS-rich" and "LS-rich" phases. The classical spinodal is then given by the solution of the following equation:

$$\frac{\partial \mu(n_{HS})}{\partial n_{HS}} = I_0\sigma_0 + k_\infty e^{-E_a/k_BT} e^{-\alpha n_{HS}}(\alpha n_{HS} - 1) = 0, \quad (2)$$

which leads to the spinodal area illustrated in the inset of Fig. 1(a).

III. COUPLED MAP MODEL

In this section we deal with the coupled map approach which allows the description of the spatiotemporal behavior of the SC solids using the simple kinetic Ising model. thus we first recall the basic grounds of the phenomenological Ising-like Hamiltonian, widely used in literature,[67] the Hamiltonian of which writes,

$$\mathcal{H} = -J\sum_{\langle i,j \rangle} s_i s_j + \sum_i \left(\Delta - \frac{k_BT}{2}\ln g\right) s_i \quad (3)$$

where, the parameter $J > 0$ is the intermolecular "ferromagneticlike" coupling between spin-crossover molecules, and s the fictitious spin with eigenvalues +1, −1 associated with the two spin states, HS, LS, respectively. Δ is the ligand field

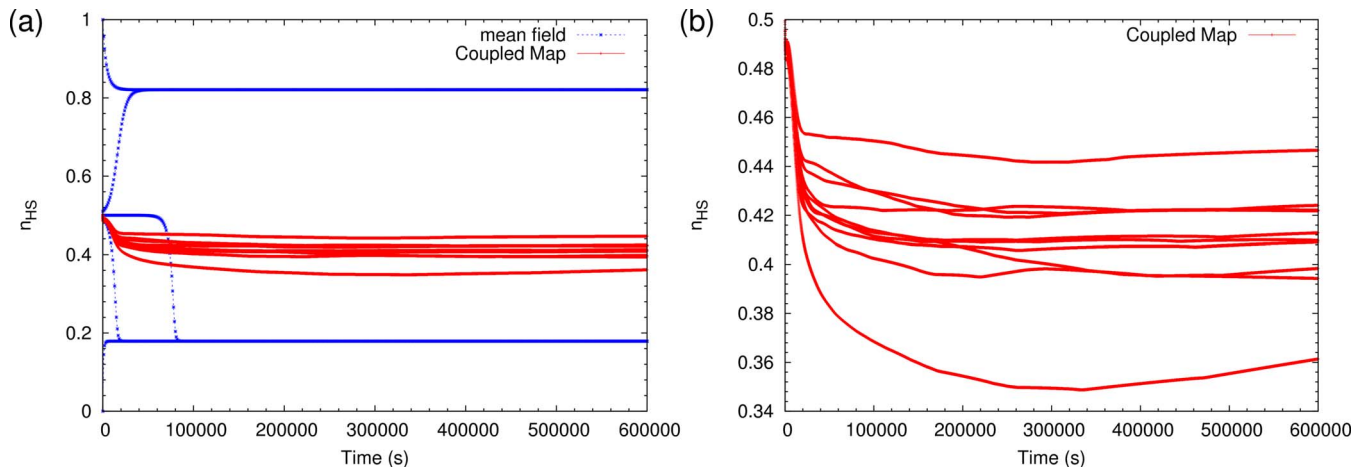

FIG. 3. (Color online) (a) Comparative mean field and coupled map results for the time evolution of the mean value of the HS fraction at $T = 53.5$ K corresponding to the center of the LITH loop of Fig. 2. All the mean-field curves converge toward the two steady states, while the coupled map curves (calculated for different initial microscopic configurations) lead to the stabilization of an intermediate state. (b) An enlarged scale of the coupled map relaxation curves of part (a) showing the existence of macroscopic fluctuations on n_{HS} attributed to the onset of short-range correlations during the self-organization process. Parameter values are given in the text.

splitting, i.e. the energy difference $E(HS)-E(LS)$ of isolated molecules, g the degeneracy ratio between the HS and LS states. The dynamics of the model is introduced in[67] following the microscopic master-equation approach

$$\frac{\partial P(\{s\};t)}{\partial t} = -\sum_{j=1}^{N} W_j(s_j|-s_j)P(\{s\}_j,s_j;t) + \sum_{j=1}^{N} W_j(-s_j|s_j\})P(\{s\}_j,-s_j;t), \quad (4)$$

where $P(\{s\};t)$ is the probability of observing the system in the configuration $(s_1,\ldots,s_N)=\{s\}$ at time t and $\frac{\partial P(\{s\};t)}{\partial t}$ is the flux of the probability, while $\{s\}_j$ denotes the configuration of all spins excepted spin s_j.

Under light, the transition rate W results from a combination of a thermal Arrhenius transition rate and an optical pumping. It writes[67] $W(s_j)=\frac{1}{2\tau_0}[(\cosh \beta E_j - s_j \sinh \beta E_j)] + \frac{I_0\sigma_0}{2}(1-s_j)$, where $E_j=-J\Sigma_i s_i+(\Delta-\frac{k_BT}{2}\ln g)$, $\frac{1}{\tau}=\frac{1}{\tau_0}e^{-\beta E_a^0}$.

The expectation value of the jth spin, defined as $\langle s_j\rangle = \Sigma_{\{s\}} s_j P(\{s\};t)$, is connected to the local HS fraction at site j as $n_j=\frac{1+\langle s_j\rangle}{2}$. In the Bragg-Williams approximation, the system probability $P(\{s\};t)$ is written as the direct product over all sites of the singlet probabilities $p(s_j;t)$, subject to $\Sigma_{s_j} p(s_j;t)=1$ for all sites. We take the singlet probability functions as the dynamic variables which describe the time evolution of the system. It is then deduced that the time dependence of the local HS fraction, at low temperature, obeys the following set of equations

$$\frac{dn_j}{dt} = I_0\sigma_0(1-n_j) - K(T)n_j \exp\left(-\alpha\sum_{k=1}^{z} n_{j+k}\right) = -\frac{\partial U}{\partial n_j}. \quad (5)$$

The frequency factor $K(T)$, is given by $K(T)=k_\infty \exp(-\beta E_a)$, where $k_\infty=2/\tau_0$ (τ_0 defines the molecular time scale of the relaxation process); the effective energy barrier $E_a = E_a^0-\Delta-zJ+\frac{k_BT}{2}\ln g$, $\alpha=J/k_BT$, and k is a subscript running over the z neighbors of site j ($j=1,N$), N being the number of molecules. The nonlinearity of the hierarchy of Eq. (5) prevents any rigorous analytical solution.

Since Hamiltonian (3) involves interactions among different sites, the distribution functions at different interacting sites are coupled to each other through the transition probabilities, leading finally to a self-consistent set of coupled differential Eq. (5). Here, we solve numerically the hierarchy of coupled differential Eq. (5) using the Runge-Kutta method, which provides a good relative accuracy ($\sim 10^{-4}$) on the local HS fraction n.

IV. RESULTS AND DISCUSSION

Let us apply the present mapped model to simulate the experimental situation of $[Fe(ptz)_6](BF_4)_2$, prepared in the spinodal region. We recall, here, that the elastic interactions as well as the crystal imperfections (such as existence of local barriers due the orientational disorder of the BF_4, and existence of dislocations upon transition) are not considered in this problem. Concretely, we prepare the system at time $t=0$ in a random state with average value $\bar{n}\simeq 0.5$. Three procedures have been used to prepare this initial state: (i) by assigning randomly the value $n_j=0$ (LS) or $n_j=1$ (HS) at each site; (ii) by distributing uniformly the probability value n_j between 0 and 1; and finally; (iii) by assigning randomly the value $n_j\simeq 0.2$ or $n_j\simeq 0.8$ (the steady-state values of the HS fraction) at each site. Then the probabilities at each site evolve following Eq. (5).

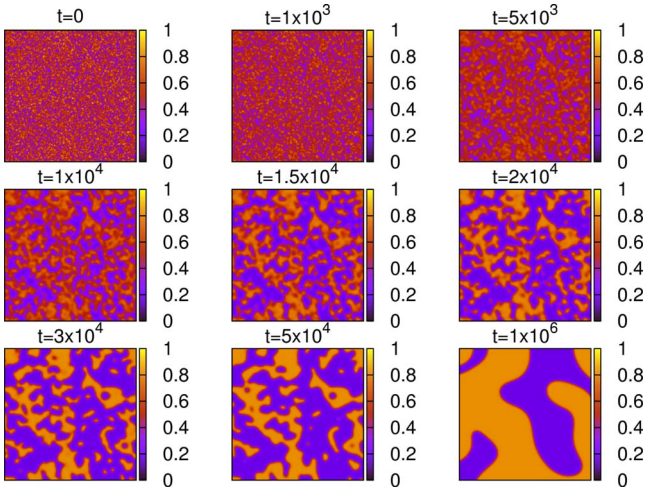

FIG. 4. (Color online) Instantaneous patterns of the HS fraction during the phase-separation process under light, starting from a homogeneous initial state at time $t=0$. The dark (yellow, colored) regions represent the rich-LS (rich-HS) phase cells. A clear evidence of self-organization of the system into spin domains is observed after $\sim 4\times 10^4$ s.

We have used the parameter values $I_0\sigma_0=5.510^{-4}$ s^{-1}, $k_\infty=1.510^{-3}$ s^{-1}, $E_a=663.5$ K, $\alpha=J/k_BT=4.7$, ($T=53.5$ K), derived from the photoexcitation and relaxation experiments on $[Fe(ptz)_6](BF_4)_2$, as already reported in Ref. 51. It is clear that the system prepared in a perfectly homogeneous initial state (equal values of the HS fraction for all sites) would merely follow the macroscopic behavior predicted by the homogeneous mean field by construction of the model.

In practice we consider a 200×200 square lattice with periodic boundary conditions, and assigned for the temperature, the value $T=53.5$ K of the transition temperature of LITH loop (see Fig. 2). The time increment was typically $\Delta t=1$ s. We have checked that lowering the time step did not alter the results, but only increased the computing time.

Figure 4 shows a typical patterning of the system, computed after an initial state made of a random distribution of n-values around the steady-state values $n\simeq 0.2$ and $n\simeq 0.8$. The onset of well-developed patterns requires $\sim 5\times 10^4$ s. The obtained structures are made of HS-rich and LS-rich areas, with local average values approaching the steady states values of Fig. 3(a) on increasing time. After 10^6 s, the patterns have coarsened to such an extent that finite-size effects can be expected.

In Fig. 5 we draw the variation of the HS fraction along the horizontal line from ($x=1$, $y=1$) to ($x=200$, $y=1$) at same times than those of Fig. 4. After 10^5 s, it is remarked that domain walls (the thickness of which is in the range

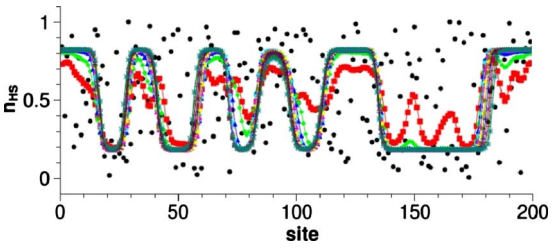

FIG. 5. (Color online) Variation of the order parameter along the horizontal line from $(x=1,\ y=1)$ to $(x=200,\ y=1)$ during the self-organization process of Fig. 4. Black dots correspond to the initial $(t=0)$ state and green squares to the configuration at time $t=5\times10^4$ s and the full lines for $t\geq10^5$ s. Well defined walls (about 10–40 sites) are formed by about 10^5 s.

10–40 sites) are formed and do not show sizable change. This defines an asymptotic behavior of the system typically beyond 10^5 s.

A. Correlation function and domain growth

We now analyze in more details the predictions of the model. It is clear that future experiments should aim to evidence the scaling laws and the structure factor which are derived in the present section. To characterize the domain-growth process, we calculate the circular averaged autostructure factor $S(k,t)$, defined by the average[68,69]

$$S(k,t)=\left\langle \sum_{\ell=1}^{N}\sum_{m=1}^{N}[n(m,t)-\bar{n}][n(\ell,t)-\bar{n}] \times\exp[-\vec{k}\,.\,(\vec{r}_m-\vec{r}_\ell)]\right\rangle, \tag{6}$$

where the wave vector is spanned over a thin circular shell in k space. In the above expression, $\bar{n}$ is the site-averaged value of $n(\ell)$, i.e., $\bar{n}=L^{-2}\Sigma_{i=1}^{L^2}n(i)$ $(L=200)$ corresponding to the macroscopic HS fraction, and the symbol average $\langle\ \rangle$ indicates an average over different runs of the number of random seeds. The typical domain size, $R(t)$, is evaluated as the inverse of the first moment of the circularly averaged structure factor, i.e.,

$$R(t)=\bar{k}(t)^{-1}=\frac{\int_0^\infty dkS(k,t)}{\int_0^\infty dkkS(k,t)}. \tag{7}$$

On the other hand, the structure factor, $S(k,t)$, scales as $S(k,t)=R(t)^d\Phi[k\times R(t)]$, where Φ is a time-independent universal function. Numerically, $\bar{k}(t)$ is computed by considering all $\vec{k}$ values up to half of reciprocal-lattice size. Thus, $\vec{k}$ take the values $\vec{k}=(2\pi\ell_x\vec{u}_x+2\pi\ell_y\vec{u}_y)/N$ (for a lattice of size $N\times N$), where ℓ_x, ℓ_y have integer values between $-\frac{N}{2}$ and $\frac{N}{2}-1$ and $\vec{u}_x$ and $\vec{u}_x$ are unit vectors in the directions x and y. It is worth noticing that even including the entire reciprocal lattice in the calculation of $\bar{k}(t)$, the results remain almost unchanged. We have evaluated the time dependence of average domain size using Eq. (7) and checked the scaling forms of the autostructure factor.

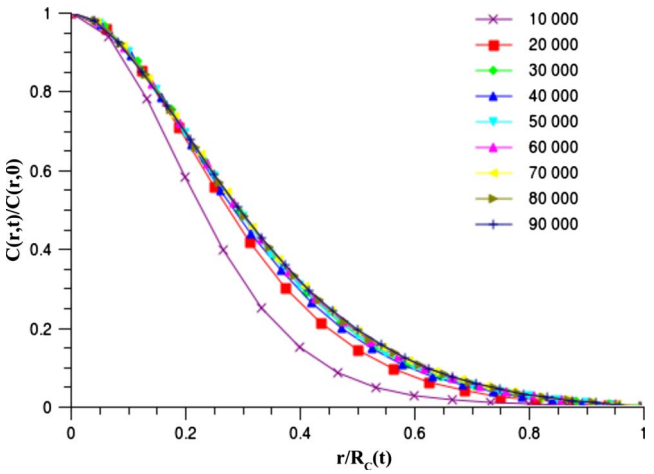

FIG. 6. (Color online) Dynamical scaling of the normalized spatial correlation function, $C(r,t)/C(0,t)$ vs $r/R_C(t)$, where $R_C(t)$ is the distance over which the correlation function falls to half its maximum value. Well defined scaling regime is obtained after 5×10^4 s.

Another important quantity which has been used to determine the domain size distribution as well as their time evolution is the real-space two points correlation function $C(r,t)$, given here by

$$C(r,t)=\langle n(\vec{\ell},t)n(\vec{\ell}+\vec{r},t)\rangle-\langle n(\vec{\ell},t)\rangle\langle n(\vec{\ell}+\vec{r},t)\rangle, \tag{8}$$

where $n(\vec{\ell},t)$ is the HS fraction at a discrete site $\vec{\ell}$ at time t; and the brackets refer to an averaging over independents runs and noise realization.

The normalized domain size distribution, $P(R(t);t)$, where $R\in[0,\infty]$ and $\int_0^\infty P(R,t)dR=1$, is obtained by examining the $n_{HS}\approx0.5$ crossings of the HS fraction profiles (shown in Fig. 5) along horizontal cross sections of the lattice.[70] In the scaling regime, the correlation function exhibits a dynamical-scaling form $C(r,t)=g(r/R)$, where the master function $g(x)$ is time independent.[70] Figure 6 superposes data from different times for $C(r,t)/C(0,t)$ vs r/R_C, where R_C is defined as the distance over which the correlation function decays to half of its maximum value. It is clearly observed that the data collapse is quite good for times $t>50\,000$. The corresponding dynamical scaling for the domain size distribution (not shown here) is $P(R,t)=R^{-1}h(R/R_P)$, where the characteristic length scale, R_P is defined from the domain distribution function as $R_P=\langle R_C\rangle$, and where a good scaling is also obtained in the late stage of the relaxation under light. It is worth noticing that in the scaling regime, R_C and R_P are equivalent up to prefactors.

We now turn to a "quantitative" discussion on the time dependence of the length scale $R(t)$ obtained either from the two points correlation (or the autostructure factor) and the domain size distribution. Our results are consistent with previous studies based on cell dynamics, Monte Carlo simulation and molecular-dynamics simulations, related to the spinodal decomposition in quenched disordered systems, using Ising Hamiltonians[71] or on two-dimensional binary fluid mixtures,[72] where it is expected that the characteristic do-

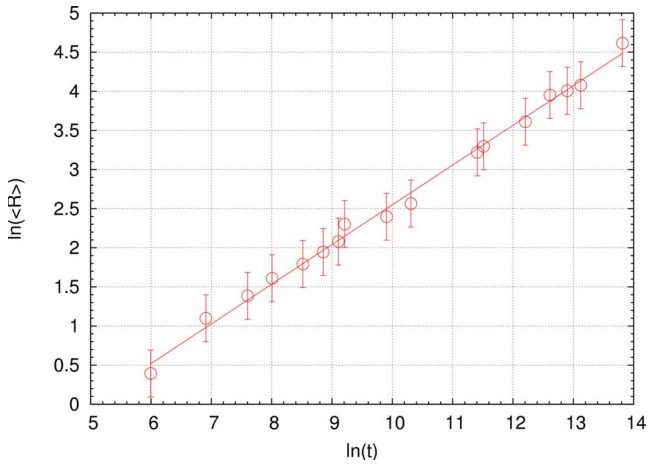

FIG. 7. (Color online) Time dependence of the logarithm of the characteristic domain length scale. The solid line is the best linear regression, giving a dynamical exponent of 0.47(0.01), which is consistent with the Allen-Cahn growth law.

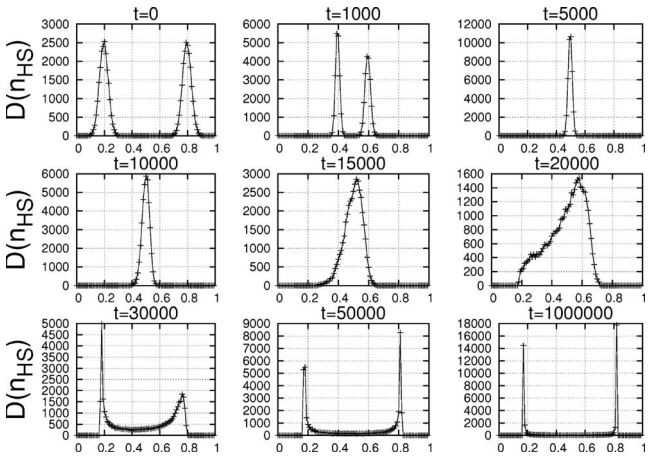

FIG. 8. Instantaneous distributions of the HS fraction corresponding to the snapshots of Fig. 4. For $t=10^6$ seconds, $D(n_{HS})$ sharply peaks around n_{HS} steady states values; a clear indication of the self-organization.

main size behaves as $\sim(t-t_0)^{1/2}$ for nonconserved order parameters.

Our results on the time evolution of the average size domain, in the scaling regime, are shown in Fig. 7. Two successive regimes have been identified as (i) a nucleation regime, for which the domain size is more or less time independent in the early stage of evolution and, (ii) an Allen-Cahn regime[71] of growth in the late stage. For the latter, we found the value $\sim 0.47 \pm 0.01$ for the dynamical growth exponent in the scaling regime, as depicted in Fig. 7. This result is consistent with the Allen-Cahn growth law[68,69] on nonconserved order parameters which gives a dynamical exponent of 1/2.

One tool helping in the understanding the microscopic mechanism governing the obtained self-organization, is the analysis of time evolution of the distribution, $D(n_{HS})$, of the HS fraction during the phase-separation process. It is worth to notice that we start here from a spatially inhomogeneous state characterized by a bimodal distribution of random values of the HS fraction distributed around the steady states $n_{HS} \simeq 0.2$ and $n_{HS} \simeq 0.8$. Incidentally, we point out that other simulations (not shown here) performed with different initial states, characterized by a Gaussian distribution around $n_{HS} \simeq 0.5$ or a flat distribution of states in the interval $n_{HS} \in [0,1]$, have led to similar results as those obtained here.

The time dependence of $D(n_{HS})$ corresponding to the snapshots of Fig. 4 is depicted in Fig. 8. The results confirm the existence of a first relaxation regime taking place during the early stage of the spinodal decomposition for times $t < 10\,000$ s, upon which the double-well structure of $D(n_{HS})$ vanishes and collapses at $\overline{n_{HS}} \simeq 0.5$, leading to the onset of a new and sharp distribution centered around $n_{HS} \simeq 0.5$.

Actually, we have identified that it corresponds to the maximum of configuration entropy, $S=-\Sigma_i p_i(t) \ln p_i(t)$, the time dependence of which is represented in Fig. 9. We point out that this regime is also partially observed in the relaxation curves of Fig. 2(a), where an initial fast relaxation regime is identified. During this fast relaxation from the inhomogeneous state (in which large concentration gradients of the HS fraction exist) to the homogeneous state, the SC cells behave quasi-independently from each other and the system follows more or less a stretched exponential relaxation. The related "domains" appear and disappear spontaneously due to thermal fluctuations and are difficult to characterize by a scaling function.

Then, as seen in Fig. 8, once the first regime is achieved, a new regime starts for which the distribution of density of states broadens and then splits, leading finally to a sharp bimodal distribution. More precisely, from $t=10^4$ s, the phase separation starts through a new regime corresponding to diffusion of interfaces, at which a broad peak located around $n_{HS} \simeq 0.5$ develops and splits. This splitting takes place at $t \simeq 3 \times 10^4$ s, and reveals a situation where the domains sizes have the same order of magnitude as that of the interfaces widths. Later on in the growth process, i.e. from $t \simeq 5 \times 10^4$ s, well formed macroscopic domains with char-

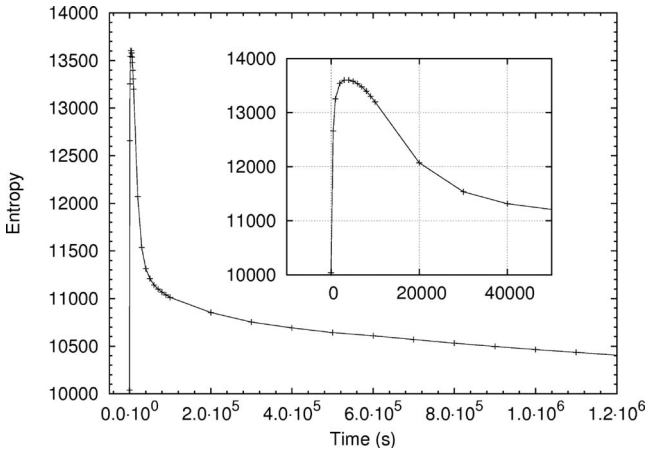

FIG. 9. Time dependence of the configuration entropy during the self-organization process. A nonmonotonic behavior is obtained corresponding to the existence of two regimes, attributed to nucleation ($t < 4 \times 10^3$ s) and domain growth ($t > 4 \times 10^3$ s).

acteristic sizes bigger than the interface widths appear, for which it corresponds a double peak distribution which becomes sharp and narrow at longer times.

Moreover, a deep examination of the time dependence of $D(n_{HS})$ indicate that the domains of the LS phase are formed after 5×10^4 s, while the domain structure of the HS the phase (dense phase) self-organize at longer time $t\simeq10^5$ s, following a regime of growth. This behavior seems to be reminiscent with that observed in the relaxations toward the LS-rich and HS-rich steady states form the respective LS and HS initial states in the homogeneous case [shown in Fig. 3(a)] where the same tendency is observed.

On the other hand, it is interesting to notice that although the utilized dynamics in the master equation was that of a nonconserved order parameter, our simulation leads to an almost constant HS fraction (up to fluctuations) during a long time interval, necessary to the phase separation, as reported in Fig. 3. This behavior can be explained by the existence of the fine balance between the optical pumping and the Arrhenius transition, slowing down the relaxation of the HS fraction, is qualitatively in good agreement with the experimental observations of magnetism under light, reported in Figs. 1(a) and 1(b).

B. Dynamic potential and driving force of spinodal decomposition

From a general point of view, phase separation has been widely investigated using phase field models[73,74] and Cahn-Hilliard equation,[75,76] introduced in the last decades. It is well known from these models that interface dynamics play a crucial role in the phase-separation process, as for example, for dendritic growth.[77–81] These classical models, such as phase field method which uses a (mesoscopic) local thermodynamic description coupling a local-order parameter to a diffusion field,[73,74] consider the problem in terms of partial differential equations, involving macroscopic quantities such as surface tension, capillary length and diffusion constants, and are efficient in describing the interfaces dynamics.

Thus, a useful approach to describe the mechanism of the present light-induced spinodal decomposition, may be obtained through an analysis of the dynamic potential $U(n)$ in the phase field approach. Let us define the field $u(\vec{r})=u(n(\vec{r}),\vec{\nabla}n(\vec{r}))$ as the dynamic potential density (similarly to the density of free energy at equilibrium) at position $\vec{r}$. The homogeneous dynamic potential, expressed as, $u(\vec{r})=u(n(\vec{r}),\vec{\nabla}n(\vec{r})=0)$, is the density of the mean-field dynamic potential given by Eq. (1). Expanding the dynamic potential density around its homogeneous value in powers of gradients, gives at the first order

$$u(n,\vec{\nabla}n)\simeq u(n,0)+\vec{\nabla}n\mathbf{K}\vec{\nabla}n \tag{9}$$

where $\mathbf{K}$ is a tensor, with components $K_{ij}=\frac{1}{2}\frac{\partial^2 u}{\partial(\partial n/\partial x_i)\partial(\partial n/\partial x_j)}$. Assuming that the dynamic potential does not depend on the gradient directions, $\mathbf{K}$ becomes a symmetric tensor. Furthermore, in the isotropic material (or cubic) that is not the case of the title compound $[Fe(ptz)_6](BF_4)_2$ which has a rhombohedral group symmetry, $\mathbf{K}$ is a diagonal tensor with equal components K. The dynamic potential density is thus approximated as

$$u(n(\vec{r}),\vec{\nabla}n(\vec{r}))=u^{\mathrm{hom}}(n)+K|\vec{\nabla}n|^2, \tag{10}$$

where K is a coefficient which is proportional to the correlation length. It is worth to notice that Eq. (10) assumes implicitly that the dynamic potential energy varies smoothly from its homogeneous value as the magnitude of the HS fraction gradient increases from zero.

Before discussing the different contributions of Eq. (10), we would like to mention that although similar developments on phase field models are widely used in literature[74,75] most of them are based on the expansion of the equilibrium free-energy functional. In contrast, in the present case, the functional $U(n(\vec{r}))$ is a nonequilibrium quantity since it contains light effect.

Equation (10) allows evaluation of the contributions to interfaces in systems that undergo spinodal decomposition, through the existence of two competing "energetic" contributions to the dynamic potential. Indeed, the gradient term in Eq. (10) tends to spread the interface region and thereby reduces the gradient as the HS fraction changes between its steady states values in adjacent phases. The first contribution $(u^{\mathrm{hom}}(n))$ derives from the increased homogeneous dynamic potential associated with the maximum of $U(n)$ [see Fig. 1(a)], which tends to narrow the interface region. Thus the simple model of Eq. (10) contains the ingredients of diffuse interfaces where the order parameter, n, varies smoothly in space from one phase to the other. The study of the rate change of the total dynamic potential, $U=\int u(n(\vec{r}),\vec{\nabla}n)dV$ (where V is the volume of the system), with respect to its current order-parameter field, $n(\vec{r};t)$ leads after some mathematical developments (assuming that the boundary integrals are negligible compared to the volume integral for large system) to the following change, δU, in the total dynamical potential when the order parameter changes by a small amount $\delta n=\dot{n}\delta t$, given by

$$\delta U=\int_V\left(\frac{\partial u^{hom}}{\partial n}-2K\nabla^2 n\right)dV=\int_V\Phi(\vec{r})dV. \tag{11}$$

Then $\Phi(\vec{r})$ the localized density of dynamic potential change due to variation in the order-parameter field, is the driving force for changing n.

This equation is the starting point for the development of the kinetic equations in the phase field approach of the present problem. Indeed, combining Eqs. (5) and (11) yields the classical Allen-Cahn equation

$$\frac{\partial n}{\partial t}=-M\left[\frac{\partial u^{hom}(n(\vec{r}))}{\partial n}-2K(n)\nabla^2 n\right], \tag{12}$$

where M is a positive kinetic coefficient related to the microscopic rearrangement kinetics. According to Eq. (12), the HS fraction n will be attracted to the local minima of u^{hom}. Depending on the initial variations in $n(\vec{r})$, the system may seek out at a rate controlled by M. The second term on the right-hand side in Eq. (12) will govern the profile of the order parameter, $n(\vec{r})$, at the antiphase boundary and will cause interfaces to move toward their center of curvatures[82]

for which $n \simeq 0.5$. This term is then at the origin of the driving force leading to the appearance of a sharp peak around the value $n_{HS} \simeq 0.5$ in the distribution $D(n_{HS})$ of Fig. 8. The first term tends to narrow the interface region and drives the phase separation.

C. Discussion

We now proceed to a general discussion on the domain growth in systems with nonconserved order parameters. The evolution of the system from an initial nonequilibrium configuration towards a final state by going through a number of intermediate states can be understood in terms of most probable paths in the phase space. The probability associated with a particular path is given by the usual statistical weight of involved configurations, which is mainly fixed by the highest-energy configuration encountered along the path. In the present case, the system is ″prepared by light″ in an initial state, with equal numbers of up and down spins randomly distributed through the lattice. The system starts ordering locally, and soon develops a number of up- and down-spin domains, competing with each other to grow. As time goes on, the number of domains decreases due to growth in size of the remaining domains. To consider this coarsening, it is instructive to consider the shrinking of a single square domain of size $L \times L$ in the case of the spin-1/2 ferromagnetic nearest-neighbor Ising model with zero-magnetic field. If we take the strength of the nearest-neighbor interaction to be J, the energy cost to flip a spin inside a LS domain is $8J$. On the boundary however, this cost is $4J$, while it is 0 at the corners of the domain. Since a corner spin can be flipped without energy cost, the most probable path for domain shrinking begins with flipping of one corner spins, which creates two new corners. This flip is followed by a random walk of the corner along an edge, each step of which has no energy cost. Thus an edge of size L is eliminated in a time proportional to L^2. In fact, this time can be calculated accurately if one considers a one dimensional random walk with probability p to jump right or left and a probability q of no jumping. The resulting analytical expression for the first-passage probability of covering a distance L in t steps is a generalization of a formula due to Lagrange,[83] which yields $t \sim L^2$ behavior even at rather small values of L. The above considerations imply a coarsening length scale $L(t) \sim t^{1/2}$, providing an equivalent way of interpreting curvature-driven growth in the present context of discrete lattice models.

An important step toward understanding growth laws in systems with nonconserved order parameter is due to Lai *et al.*,[84] who proposed four classes of systems, determined by the dependence of the energy barrier to coarsening on the characteristic domain length. The growth of the domains is driven by a curvature-reduction mechanism as

$$\frac{dL(t)}{dt} = \frac{a(L,T)}{L(t)}, \tag{13}$$

where the diffusion constant $a(L,T)$ depends on the domain scale L and temperature. Two cases are interesting to quote:

(1) for systems for which $a(L,T)$ is independent of L and remains nonzero as $T \to 0$, there exists relaxation paths that have no energy barrier and the nature of the relaxation does not depend on the coarsening length scale. The Ising model with usual Glauber or Metropolis transition rates clearly belongs to this first case. In general, $L(t) \sim t^{1/2}$ for this class of systems.

(2) In the Ising-like model with local energy barriers (Arrhenius transition rates), although the minimum-energy barriers are again independent of L, the elementary diffusion process (a corner moving along an edge) has a local energy barrier E_a^0, so that $a(L,T) = a_0 \exp(-E_a^0/k_B T)$. In this case, we also obtain a $t^{1/2}$ law, but with a time scale $\tau = \tau_0 \exp(-E_a^0/k_B T)$. It is clear from the above equation that domain growth will be slow for this type of systems with $L(t)$ constant for times $t \ll \tau$, where $\tau \simeq 4000$ s in the present study. For larger times, the growth law is $L(t) \sim (t/\tau)^{1/2}$, corresponding to the Allen-Cahn law. These predictions are in good agreement with the behavior extracted from our numerical simulations.

V. SUMMARY AND CONCLUSION

In summary, we presented a dynamic coupled map method for ″simulating″ dynamic process of light-induced phase separation in SC solids under permanent irradiation. The method is based on a microscopic model describing the SC system, combined with a master equation governing the time evolution of the probability distribution functions for lattice models. Its effectiveness lies in the fact that (i) the equations of motion find again the well-known macroscopic equation already used to describe the homogeneous system, and (ii) it allows description of the phase separation under light as well as the spatial behavior of the HS fraction during the spinodal decomposition process. In our best knowledge, this is a first time where such problem is addressed in the field of SC studies. In addition, although we restricted our studies to the low-temperature region, the model can be naturally extended to the description of the spatial dependence of the HS fraction in case of equilibrium first-order transition, accompanied with a hysteresis loop. At the beginning of this paper, we mentioned that one of the motivations of this work was to propose a microscopic model for describing the light-induced phase-separation process in SC solids, avoiding the macroscopic phase field descriptions, such as time-dependent Ginzburg-Landau models. However, it was possible to demonstrate that the discrete scheme of evolution Eq. (5) can be connected with well-known field-theoretic models[85] through a generalized expression of Eq. (12). A more detailed study on these aspects, necessary to calculate the dynamics of the interface and their structure will be published elsewhere.

As closing remarks, we discuss briefly the limitations of the local dynamic mean-field approximations. First, it shares all the pitfalls of mean field since it neglects the fluctuations. Thus it is quite inappropriate to apply such method to the critical region or other situations where fluctuations dominate the dynamics. Usually for most domain-growth processes resulting from a deep thermal quenching of the system, the effect of fluctuations are not important and the domain growth is dominated by the nonlinearity of the dynamics. That is not the case for systems quenched under

light,[51] where the combination of the slow relaxation of the order parameter and the fluctuations of the intensity of light may induce important features in the dynamics, like the Barkhausen noise.[51] To tackle such problems, it is necessary to extend the present approach by adding, for example, a conservative Langevin noise contribution, which can be inserted in kinetic Eq. (5). It is expected that noise changes the interface profiles (side branches may develop for example) as well as their dynamics. That is the next target of this work.

ACKNOWLEDGMENTS

The authors wish to thank S. Miyashita for helpful discussion. This work was supported by European Network of Excellence MAGMANET (Grant No. FP6-515767-2), Conseil Régional d'Ile de France, CNRS, Université de Versailles Saint-Quentin and PPF contract from the ″'Ministère de l'Enseignement Supérieur et de la Recherche.″

*kbo@physique.uvsq.fr

[1] S. Koshihara, Y. Tokura, K. Takeda, and T. Koda, Phys. Rev. Lett. **68**, 1148 (1992).
[2] K. Miyano, T. Tanaka, Y. Tomioka, and Y. Tokura, Phys. Rev. Lett. **78**, 4257 (1997).
[3] N. Takubo, I. Onishi, K. Takubo, T. Mizokawa, and K. Miyano, Phys. Rev. Lett. **101**, 177403 (2008).
[4] S. Iwai, S. Tanaka, K. Fujinuma, H. Kishida, H. Okamoto, and Y. Tokura, Phys. Rev. Lett. **88**, 057402 (2002).
[5] O. Sato, T. Iyoda, A. Fujishima, and K. Hashimoto, Science **272**, 704 (1996).
[6] Y. Moritomo *et al.*, Phys. Rev. B **68**, 144106 (2003).
[7] T. Yamauchi, A. Nakamura, Y. Moritomo, T. Hozumi, K. Hashimoto, and S. Ohkoshi, Phys. Rev. B **72**, 214425 (2005).
[8] Y. Moritomo, F. Nakada, H. Kamioka, T. Hozumi, and S. Ohkoshi, Phys. Rev. B **75**, 214110 (2007).
[9] Y. Tokura, *Colossal Magnetoresistive Oxides* (Gordon and Breach, New York, 2000).
[10] S. Sridevi, S. K. Prasad, and G. G. Nair, Phys. Rev. E **80**, 021703 (2009).
[11] K. Koshino and T. Ogawa, Phys. Rev. B **58**, 14804 (1998).
[12] K. Ishida and K. Nasu, Phys. Rev. B **76**, 014302 (2007).
[13] K. Ishida and K. Nasu, Phys. Rev. Lett. **100**, 116403 (2008).
[14] K. Ishida and K. Nasu, Phys. Rev. B **77**, 214303 (2008).
[15] Y. Ogawa, S. Koshihara, K. Koshino, T. Ogawa, C. Urano, and H. Takagi, Phys. Rev. Lett. **84**, 3181 (2000).
[16] Y. Moritomo, M. Kamiya, A. Nakamura, A. Nakamoto, and N. Kojima, Phys. Rev. B **73**, 012103 (2006).
[17] F. Varret, K. Boukheddaden, A. Goujon, B. Gillon, and G. McIntyre, Z. Kristallogr. **223**, 250 (2008).
[18] W. Nicolazzi, S. Pillet, and C. Lecomte, Phys. Rev. B **78**, 174401 (2008).
[19] P. Gütlich, Struct. Bonding (Berlin) **44**, 83 (1981).
[20] O. Kahn and J. P. Launay, Chemtronics **3**, 140 (1988).
[21] J. Jeftic and A. Hauser, J. Phys. Chem. B **101**, 10262 (1997).
[22] G. Molnár, V. Niel, J.-A. Real, L. Dubrovinsky, A. Bousseksou, and J. J. McGarvey, J. Phys. Chem. B **107**, 3149 (2003).
[23] S. Decurtins, P. Gütlich, C. P. Köhler, H. Spiering, and A. Hauser, Chem. Phys. Lett. **105**, 1 (1984).
[24] P. Gütlich, A. Hauser, and H. Spiering, Angew. Chem., Int. Ed. Engl. **33**, 2024 (1994).
[25] S. Bonhommeau, G. Molnár, A. Galet, A. Zwick, J.-A. Real, J. J. McGarvey, and A. Bousseksou, Angew. Chem., Int. Ed. **44**, 4069 (2005).
[26] N. O. Moussa, G. Molnár, S. Bonhommeau, A. Zwick, S. Mouri, K. Tanaka, J. A. Real, and A. Bousseksou, Phys. Rev. Lett. **94**, 107205 (2005).
[27] S. Decurtins, P. Gütlich, K. M. Hasselbach, A. Hauser, and H. Spiering, Inorg. Chem. **24**, 2174 (1985).
[28] A. Bousseksou, K. Boukheddaden, M. Goiran, C. Conséjo, M.-L. Boillot, and J. P. Tuchagues, Phys. Rev. B **65**, 172412 (2002).
[29] E. König, Struct. Bonding. (Berlin) **76**, 51 (1991).
[30] O. Kahn, Curr. Opin. Solid State Mater. Sci. **1**, 547 (1996).
[31] J. Krober, E. Codjovi, O. Kahn, F. Grolire, and C. Jay, J. Am. Chem. Soc. **115**, 9810 (1993).
[32] B. Gallois, J.-A. Real, C. Hauw, and J. Zarembowitch, Inorg. Chem. **29**, 1152 (1990).
[33] E. W. Mueller, J. Ensling, H. Spiering, and P. Gütlich, Inorg. Chem. **22**, 2074 (1983).
[34] G. Vos, R. A. L. Febre, R. A. G. de Graff, J. G. Haasnoot, and J. Reedijk, J. Am. Chem. Soc. **105**, 1682 (1983).
[35] E. Koenig, G. Ritter, S. Kulshreshtha, J. Waigel, and H. Goodwin, Inorg. Chem. **23**, 1896 (1984).
[36] E. Koenig, G. Ritter, H. Grnsteudel, J. Dengler, and J. Nelson, Inorg. Chem. **33**, 837 (1994).
[37] V. Ksenofontov, H. Spiering, A. Schreiner, G. Levchenko, H. Goodwin, and P. Gütlich, J. Phys. Chem. Solids **60**, 393 (1999).
[38] A. Bousseksou, G. Molnàr, P. Demont, and J. Menegotto, J. Mater. Chem. **13**, 2069 (2003).
[39] Y. Garcia, V. Ksenofontov, and P. Gütlich, Hyperfine Interact. **139-140**, 543 (2002).
[40] O. Kahn and E. Codjovi, Philos. Trans. R. Soc. London, Ser. A **354**, 359 (1996).
[41] E. Freysz, S. Montant, S. Létard, and J.-F. Létard, Chem. Phys. Lett. **394**, 318 (2004).
[42] O. Kahn, *Molecular Magnetism* (VCH, New York, 1993).
[43] S. Decurtins, P. Gütlich, C. Köhler, and H. Spiering, Chem. Phys. Lett. **1**, 139 (1984).
[44] A. Hauser, Coord. Chem. Rev. **111**, 275 (1991).
[45] A. Hauser, Comments Inorg. Chem. **17**, 17 (1995).
[46] A. Desaix, O. Roubeau, J. Jeftic, J. G. Haasnoot, K. Boukheddaden, E. Codjovi, J. Linarès, M. Nogues, and F. Varret, Eur. Phys. J. B **6**, 183 (1998).
[47] J.-F. Létard, P. Guionneau, L. Rabardel, J. A. K. Howard, A. E. Goeta, D. Chasseau, and O. Kahn, Inorg. Chem. **37**, 4432 (1998).
[48] F. Varret, K. Boukheddaden, J. Jeftic, and O. Roubeau, Mol. Cryst. Liq. Cryst. **335**, 561 (1999).
[49] E. W. Müller, H. Spiering, and P. Gütlich, J. Chem. Phys. **79**, 1439 (1989).
[50] K. Ichiyanagi, J. Hebert, L. Toupet, H. Cailleau, P. Guionneau, J.

F. Létard, and E. Collet, Phys. Rev. B **73**, 060408(R) (2006).
[51] F. Varret, K. Boukheddaden, C. Chong, A. Goujon, B. Gillon, J. Jeftic, and A. Hauser, EPL **77**, 30007 (2007).
[52] A. Goujon, F. Varret, K. Boukheddaden, C. Chong, J. Jeftic, Y. Garcia, A. D. Naik, J. Ameline, and E. Collet, Inorg. Chim. Acta **361**, 4055 (2008).
[53] Y. Moritomo, K. Kato, A. Kuriki, A. Nakamoto, N. Kojima, M. Takata, and M. Sakata, J. Phys. Soc. Jpn. **71**, 2609 (2002).
[54] M. Hanawa, Y. Morimoto, A. Kuriki, J. Tateishi, K. Kato, M. Takata, and M. Sakata, J. Phys. Soc. Jpn. **72**, 987 (2003).
[55] S. Pillet, J. Hubsch, and C. Lecomte, Eur. Phys. J. B **38**, 541 (2004).
[56] N. Huby, L. Guérin, E. Collet, L. Toupet, J. C. Ameline, H. Cailleau, T. Roisnel, T. Tayagaki, and K. Tanaka, Phys. Rev. B **69**, 020101(R) (2004).
[57] J.-F. Létard, P. Guionneau, O. N'Guyen, J. Sanchez Costa, S. Marcén, G. Chastanet, M. Marchivie, and L. Goux-Capes, Chem.-Eur. J. **11**, 4582 (2005).
[58] S. Pillet, V. Legrand, M. Souhassou, and C. Lecomte, Phys. Rev. B **74**, 140101(R) (2006).
[59] M. Avrami, J. Chem. Phys. **7**, 1103 (1939).
[60] M. Avrami, J. Chem. Phys. **8**, 212 (1940).
[61] A. Goujon, B. Gillon, A. Debede, A. Cousson, A. Gukasov, J. Jeftic, G. J. McIntyre, and F. Varret, Phys. Rev. B **73**, 104413 (2006).
[62] O. Sakai, T. Ogawa, and K. Koshino, J. Phys. Soc. Jpn. **71**, 978 (2002).
[63] O. Sakai, M. Ishii, T. Ogawa, and K. Koshino, J. Phys. Soc. Jpn. **71**, 2052 (2002).
[64] C. Enachescu, L. Stoleriu, A. Stancu, and A. Hauser, Phys. Rev. Lett. **102**, 257204 (2009).
[65] S. Miyashita, P. A. Rikvold, T. Mori, Y. Konishi, M. Nishino, and H. Tokoro, Phys. Rev. B **80**, 064414 (2009).
[66] W. Nicolazzi, S. Pillet, and C. Lecomte, Phys. Rev. B **80**, 132102 (2009).
[67] K. Boukheddaden, I. Shteto, B. Horomano, and F. Varret, Phys. Rev. B **62**, 14806 (2000).
[68] Z. G. Wang, Phys. Rev. A **45**, 692 (1992).
[69] Y. Oono and S. Puri, Phys. Rev. A **38**, 434 (1988).
[70] K. Binder and D. Staufer, Phys. Rev. Lett. **33**, 1006 (1974).
[71] R. Paul, S. Puri, and H. Rieger, Phys. Rev. E **71**, 061109 (2005).
[72] A. Thakre, W. den Otter, and W. Riels, Phys. Rev. E **77**, 011503 (2008).
[73] A. A. Wheeler, W. J. Boettinger, and G. B. McFadden, Phys. Rev. E **47**, 1893 (1993).
[74] J. Langer and R. Sekerka, Acta Metall. Mater. **23**, 1225 (1975).
[75] J. Cahn and J. Hilliard, J. Chem. Phys. **28**, 258 (1958).
[76] J. Cahn, Acta Metall. Mater. **9**, 795 (1961).
[77] M. Plapp and J. Gouyet, Phys. Rev. E **55**, 45 (1997).
[78] M. Plapp and J. F. Gouyet, Phys. Rev. E **55**, 5321 (1997).
[79] J. S. Langer, Rev. Mod. Phys. **52**, 1 (1980).
[80] D. Kessler, J. Koplik, and H. Levine, Adv. Phys. **37**, 255 (1988).
[81] Y. Pomeau and M. B. Amar, in *Solids Far from Equilibrium*, edited by C. Goderèche (Cambridge University Press, Cambridge, 1992).
[82] S. Allen and J. Cahn, Acta Metall. Mater. **27**, 1085 (1979).
[83] K. Tafa, S. Puri, and D. Kumar, Phys. Rev. E **63**, 046115 (2001).
[84] Z. W. Lai, G. F. Mazenko, and O. T. Valls, Phys. Rev. B **37**, 9481 (1988).
[85] P. Hohenberg and B. Halperin, Rev. Mod. Phys. **49**, 435 (1977).